A SEGMENTATION METHOD USING COMPOUND MARKOV RANDOM FIELDS BASED ON A GENERAL BOUNDARY MODEL

Jue Wu and Albert C.S. Chung

Bioengineering Program and Department of Computer Science, School of Engineering,
The Hong Kong University of Science and Technology, Hong Kong.

ABSTRACT

Markov random field (MRF) theory has widely been applied to segmentation in noisy images. This paper proposes a new MRF method. First, it couples the original labeling MRF with a boundary MRF that can help improve the performance of segmentation. Second, the boundary model is general and does not need prior training. Third, unlike existing related work, our model offers more compact interaction between the two MRFs. Experiments on synthetic images and real clinical datasets show that the proposed approach is able to produce good segmentation results, especially removing noise in low signal-to-noise ratio regions.

1. INTRODUCTION

To tackle the difficult problem of image segmentation, researchers have proposed a variety of methods, one of which is the Markov random fields (MRF). When the concept was first introduced into the field of statistical image analysis in middle 1980's, Geman and Geman [1] and Besag [2] applied MRF to image restoration which is closely related to segmentation. Unlike [2] that used a single labeling MRF, we incorporate another MRF (boundary MRF) to represent the boundary of a region and thus construct a compound MRF model. Similar to [1], Geiger *et al*. [3] also added a second MRF (line process) for surface reconstruction. However, our boundary MRF is different from line process in the sense that we define the MRF not on dual lattice between pixels but on the pixel site directly. Moreover, the two MRFs in our model interact more sophisticatedly while the line process works implicitly [4] and is relatively simple.

In general, adopting two or more MRFs in one task is to solve two or more different problems. For example, Sun *et al*. [5] integrated three MRFs, disparity, line process and occlusion, because these three factors are all critical to stereo matching. Likewise, Arduini *et al*. [6] solved two problems, restoration of SAR images and extraction of intensity discontinuities, by using two MRFs. Our current model aims at segmentation problem alone with incorporation of boundary MRF in order to improve its performance. Although Held *et al*. [7] also used one added MRF, i.e. the bias field, to sweep the obstacle of MRI segmentation, they did not couple the two MRFs as compactly as ours because they assumed the two fields were independent.

In this paper, we propose a more compactly interacting model to help the original labeling MRF. The novel model takes into consideration the relationship of the regions and their boundaries. We construct the interaction of the two MRFs in a neighborhood by preferring a series of patterns and penalizing the other situations with the basic assumption that true boundaries should be linked and matched with labeling patterns reasonably while discontinuities caused by random noise are not. In the experiments, we synthesize a number of simulated images with different signal-to-noise ratios (SNR) to test our method. Besides, by applying the approach to real medical data, we find the new model can significantly reduce the number of false positives of segmentation while preserving the extracted objects.

2. MODEL FORMULATION

2.1. The MAP-MRF framework

Advocated by Geman and Geman [1], maximum *a posterior* (MAP) is usually used to estimate the MRF solution. Let $S = \{1, ..., n\}$ index n sites in an image lattice. $X = \{x_i | i \in S\}$ and $D = \{d_i | i \in S\}$ are both MRFs representing labels and boundary tags, respectively. x_i is one of the labels in $L_1 = \{0, 1, ..., m-1\}$ where m is the number of possible classes. d_i is one of the tags in $L_2 = \{0, 1\}$, where 0 and 1 represent non-boundary and boundary sites, respectively. The observed field is denoted by $Y = \{y_i | i \in S\}$, where y_i is the observed image intensities. Let $\Omega_X = L_1 \times \cdots \times L_1 = L_1^n$ and $\Omega_D = L_2 \times L_2 = L_2^2$ be the configuration spaces of X and D, respectively.

The posterior probability $P(X, D|Y)$ can be estimated by the Bayesian theorem, $P(X, D|Y) \propto P(Y|X, D) \times P(X, D)$, where $P(Y|X, D)$ reflects the likelihood of observed data given the information of label and boundary, and $P(X, D)$ embodies prior knowledge of the two MRFs. The MAP estimation for the optimal solution is expressed by

$$(\hat{X}, \hat{D}) = \arg \max_{X \in \Omega_X, D \in \Omega_D} P(Y|X, D)P(X, D). \quad (1)$$

0-7803-9134-9/05/$20.00 ©2005 IEEE

By virtue of the Markovianity of MRF theory, interactions between sites in S are constrained in a neighborhood system $N = \{N_i | i \in S\}$, where $N_i \subseteq S$ denotes a set of sites in the vicinity of site i. According to the Hammersley-Clifford theorem, the MAP estimation can become

$$(\hat{X}, \hat{D}) = \arg \max_{X \in \Omega_X, D \in \Omega_D} \frac{1}{Z} e^{-\frac{U(Y|X,D)+U(X,D)}{T}}, \quad (2)$$

where Z is a normalizing constant, $U(Y|X,D)$ and $U(X,D)$ are the likelihood and prior energy function, respectively. It further leads to an energy minimization problem, that is,

$$(\hat{X}, \hat{D}) = \arg \min_{X \in \Omega_X, D \in \Omega_D} (U(Y|X,D) + U(X,D)), \quad (3)$$

where $\hat{X}$ is the solution to the segmentation problem. We assume Y and D are independent of each other because the observed image intensity is not affected whether the site is on the region boundary or inside the region. Therefore, the likelihood energy becomes $U(Y|X,D) = U(Y|X)$. Assuming that each region is nearly homogeneous before it is added by a Gaussian noise with zero mean and standard deviation σ, we can formulate the likelihood energy as $U(Y|X) = \sum_{i \in S} \sum_{j=0}^{m-1} \delta(x_i - j) \cdot \frac{(y_i - \mu_j)^2}{2\sigma^2}$, where if $x = 0$, $\delta(x) = 1$, else $\delta(x) = 0$, and μ_j represents the mean intensity of region j.

2.2. Coupling labeling MRF with boundary MRF

d_i	$\sum_{j \in N_i} d_j$	$\sum_{j \in N_i} x_i \oplus x_j$
0	0(0)	0(0)
0	1(1)	0(0)
0	2(2)	0(0)
0	2(4)	2(4)
1	2(4)	1(1)
1	2(4)	2(2)
1	3(5)	1(1)
1	3(5)	2(2)
1	4(6)	1(2)
1	4(6)	3(3)

Table 1. *For 2D and 3D scenarios, this table lists all preferred configurations of two coupled MRFs, X and D. Numbers in parentheses are for 3D scenario.*

The prior energy $U(X,D)$ defines the interaction between the two MRFs, X and D, and is the major contribution of this paper. Here we adopt a general model that does not need prior training about the boundary patterns. We pick a number of preferable cases from all the possible combinations of X and D configurations in N and penalize other cases. For 2D scenario and 1^{st} order Ising neighborhood system, the guidance rules are listed in Table 1. These are all preferred combinations of x_i, d_i and their neighborhood. Each row represents one case that should be assigned a low energy value. Those configurations of the two MRFs that are not in the list should be penalized and assigned a high energy. Therefore, we get our new prior energy formulation

$$U(X,D) = \sum_{i \in S} \gamma \cdot \Big[\delta(d_i) T_1 + \delta(d_i - 1) T_2\Big], \gamma > 0, \quad (4)$$

$$T_1 = \Big(\sum_{j \in N_i} x_i \oplus x_j + \sum_{j \in N_i} d_j \cdot | \sum_{j \in N_i} d_j - 1| \cdot | \sum_{j \in N_i} d_j - 2| \Big) \cdot \Big(| \sum_{j \in N_i} x_i \oplus x_j - 2| + | \sum_{j \in N_i} d_j - 2| \Big),$$

$$T_2 = \Big(| \sum_{j \in N_i} x_i \oplus x_j - 1| \cdot | \sum_{j \in N_i} x_i \oplus x_j - 2| + | \sum_{j \in N_i} d_j - 2| \cdot | \sum_{j \in N_i} d_j - 3| \Big) \cdot \Big(| \sum_{j \in N_i} x_i \oplus x_j - 1| \cdot | \sum_{j \in N_i} x_i \oplus x_j - 3| + | \sum_{j \in N_i} d_j - 4| \Big),$$

where $\oplus$ represents the "exclusive or" operation and γ is the penalty. Terms T_1 and T_2 account for non-boundary ($d_i = 0$) and boundary ($d_i = 1$) situations, respectively. For example, in Table 1, if the conditions of the second row are satisfied, T_1 will be zero and a low prior energy is obtained.

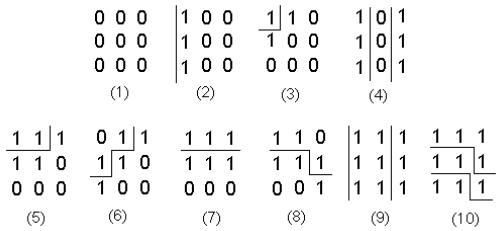

Fig. 1. *Preferred 3×3 neighborhood configuration of the boundary MRF D. The central site corresponds to d_i. Only four neighbors are considered in MRF if 1^{st} order Ising model is used. These patterns include occasions absent of edge (1), adjacent to a straight edge (2)(7), adjacent to an edge corner (3)(5), present of one-pixel wide region (4)(10), present of a diagonal edge (6)(8), present of two-pixel wide region (9).*

Fig. 1 illustrates why the prior energy definition in Eq. 4 and the preferred situations in Table 1 make sense. Subfigures (1)-(10) in Fig. 1 correspond to the 2nd to 11th rows in Table 1. These 3×3 neighborhood sites are all boundary MRF configurations. Between two boundaries of two regions is the edge which is represented by lines. In other words, on one side of the edge is the region that is different from the other side. These configurations of boundary MRF, D, restrict the corresponding labeling MRF, X, within some patterns. Details can be found in the caption of Fig. 1. Notice that we adopt the 1^{st} order Ising model for the sake of less computational cost. Also note that the formulation in Eq. 4 is rotation invariant.

The motivation to use this model is that true boundary or edge without noise should be continuous at least in a small area, like 3×3 neighborhood. If one site is corrupted by

noise and regarded as boundary, probably the neighborhood will not conform to the true pattern of linked boundary because of the randomness of noise. Then due to the penalty given by the prior energy term, this case will be discarded. In Sec. 3, more details will be given on the experimental justification of choosing these ten patterns.

The extension from 2D to 3D is straightforward. The neighboring sites increase from 4 to 6. Numbers with parentheses in Table 1 represent the preferred cases concerning the configurations of X and D. The 3D prior energy function can be given similarly as Eq. 4.

3. EXPERIMENTAL RESULTS

In the experiments, although we focus on the binary segmentation i.e. $m = 2$ for X labeling set L_1, implementations for multi-class segmentation are exactly the same. Binary segmentation has one challenging application that is the extraction of blood vessels from vascular images.

3.1. Synthetic data

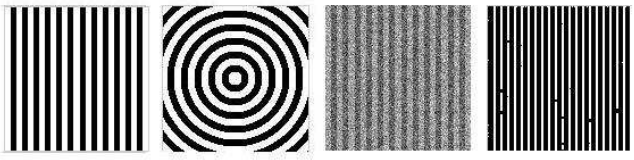

Fig. 2. *The first and second subfigures are synthetic images with straight bars and circular tubes. The third and fourth are examples of noisy images and resulting boundary MRF, D.*

We construct two types of simulated data in the experiments. One consists of straight bars and the other consists of circular tubes. The 2D synthetic images are 128×128 in size and have the width of 3 and 6 pixels which represent average small and large blood vessels, respectively (Fig 2). Before noise is added to these ground truth data, we first verify that the ten patterns chosen in the model are typical in images. We count the frequencies of these patterns in different simulated images with various object orientations and widths. Results are listed in Table 2, which shows that the ten patterns in our model represent the majority.

To mimic the true environment of real data, we corrupt each synthetic image with Gaussian noise having zero mean and same standard deviations (SD) following the style in our previous work [8]. We try different SDs to produce corrupted images with different signal-to-noise ratios (SNR). SNR is calculated by $(\mu_o - \mu_b)/\sigma$, where μ_o and μ_b are the true intensities of object and background, and σ represents the SD of the added noise. In the experiments, $\mu_o = 160$ and $\mu_b = 100$.

To evaluate the performance of the proposed method, we compare it with three other common MRF methods based on these synthetic images. The first method is to use a single

	90°	60°	45°	30°	0°	circle
3	100%	93.65%	100%	93.65%	100%	95.84%
6	100%	100%	100%	100%	100%	100%

Table 2. *Percentages of the ten patterns occurring in simulated data (width = 3 for the second row, width = 6 for the third row). The second to sixth columns are for straight bars of different orientations and the seventh column is for circular tubes.*

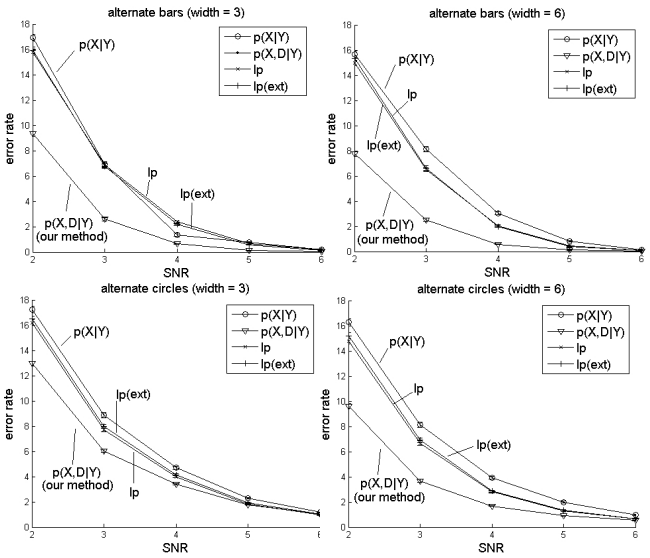

Fig. 3. *The function of error rate of 4 models over various SNRs.*

MRF, X, for the segmentation and have the same prior energy definition without bias field as in [7] (**P(X|Y)** in Fig.3). The second method [1] makes use of the line process (**lp** in Fig.3). The third method [3] adopts line process with more interaction between discontinuity sites (**lp(ext)** in Fig.3). These three methods are the same as our model in terms of the likelihood function. The difference between these models and ours lies in the prior function which embodies the interaction between sites. Please refer to [1, 3, 7] for more details of the definitions. Comparison results are plotted in Fig.3, where our method is represented as **P(X,D|Y)**.

We optimize all four MRF formulations by the iterated conditional modes (ICM) algorithm [2]. ICM is an efficient deterministic solver for MRF. However, ICM will reach a local optimum because it is gradient descendant. We once tried to use other more global methods to solve our model, e.g. belief propagation. Unfortunately, because the prior energy in our model is not pair-site defined, belief propagation and other variants are not applicable. Besides, graph cut method is not suitable to our model because the prior energy function is not regular [9].

The error rate of the segmentation is given by: (The number of misclassified pixels / The total number of pixels in the image)$\times 100\%$. The initial X is obtained by the maximum likelihood estimate [4] $X^{(0)} = \arg\max_{X \in \Omega_X} P(Y|X)$

and the initial D can be set by specifying a threshold to differentiate between boundary and non-boundary pixels. All the parameters in the likelihood functions are known for the simulated images. We repeat each experiment for ten times, calculate the means and SDs, and plot error rates of four methods over different SNRs in Fig. 3. The results show that when the SNR is low (e.g. 2 or 3), our model can significantly improve the accuracy of the segmentation compared to the other three models.

3.2. Real data

We apply our method to clinical vascular datasets and compare the results with the single MRF model. In vascular images, blood vessels are inhomogeneous in intensity especially in the region which clinicians are interested in, e.g. aneurysm. This brings difficulties to segmentation. For example, the conventional single MRF (as described in Section 3.1) seems to suffer from a large amount of false positive pixels due to the low SNR.

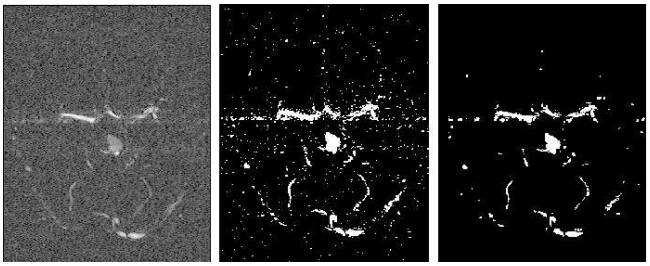

Fig. 4. *Results of two methods on PCMRA images. From left to right are the original image, segmented image of the single MRF model and segmented image of our model.*

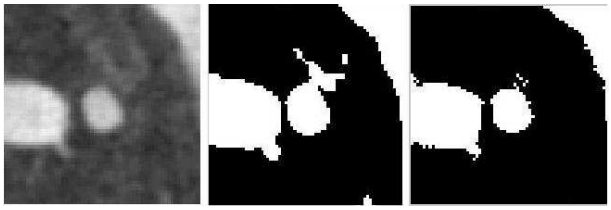

Fig. 5. *Results of two methods on 3DRA images (region of interest). From left to right are the original image, segmented image of the single MRF model and segmented image of our model.*

We performed experiments on five phase contrast magnetic resonance angiography (PCMRA) images (512×512) and one three dimension rotational angiography (3DRA) image ($128 \times 128 \times 128$). The initializations of X and D are the same as in the synthetic data experiments. We estimate the values of μ_o and μ_b by selecting the regions of interest (ROIs) in foreground and background, respectively. (More automatic estimation methods like EM [8] can be used in the future.) Fig.4 shows the comparison results of the two methods on PCMRA data. The single MRF model suffered from the high noise level and oversegmented the background whereas the proposed method could reduce the number of noisy pixels to a low level in the segmented image. Fig.5 shows the results on 3DRA. Notice the false segmented region protruding from the central blood vessel in the middle subfigure. Conversely, the proposed method could avoid extracting noisy spurious regions.

Experiments on synthetic and real images show the proposed approach can outperform the conventional methods because it has the advantages of 1) taking into consideration the discontinuity between different regions while a single MRF does not [7]; 2) allowing the interaction between d_i and its neighbors d_j, which does not exist in [1]; 3) interacting between boundary neighborhood and labeling neighborhood in a more intensive way than the work of [3].

4. SUMMARY

In this paper, we propose a new method using compound MRFs based on a general boundary model. The main target of this approach is to enhance the performance of segmentation by emphasizing the relationship between labeling and boundary. The experiments and comparisons with other existing MRF methods show that the proposed model can give good segmentation results in high noise level regions.

5. REFERENCES

[1] S.Geman and D.Geman, "Stochastic relaxation, gibbs distribution and the bayesian restoration of images," *IEEE Trans. PAMI*, vol. 6, no. 6, pp. 721–741, 1984.

[2] J.Besag, "On the statistical analysis of dirty pictures," *Journ. of the Roy. Stat. Soc.*, vol. Series B 48, pp. 259–302, 1986.

[3] D.Geiger and F.Girosi, "Parallel and deterministic algorithm from mrf's: surface reconstruction," *IEEE Trans. PAMI*, vol. 13, pp. 401–412, 1991.

[4] S.Z.Li, Ed., *Markov Random Field Modeling in Image Analysis*, Springer-Verlag Tokyo, 2001.

[5] J.Sun, N.Zheng, and H.Shum, "Stereo matching using belief propagation," *IEEE Trans. PAMI*, vol. 25, pp. 787–800, 2003.

[6] F.Arduini, C.Dambra, and C.S.Regazzoni, "A coupled mrf model for sar image restoration and edge-extraction," in *Int. Geosci. Remote Sensing Symp.*, 1992, vol. 2, pp. 1120–1122.

[7] K.Held *et al*, "Markov random field segmentation of brain mr images," *IEEE TMI*, vol. 16, pp. 878–886, 1997.

[8] A.C.S.Chung, J.A.Noble, and P.Summers, "Vascular segmentation of pcmra based on statistical mixture modeling and local phase coherence," *IEEE TMI*, vol. 23, pp. 1490–1507, 2004.

[9] V.Kolmogorov and R.Zabih, "What energy functions can be minimized via graph cuts?," *IEEE Trans. PAMI*, vol. 26, pp. 147–159, 2004.